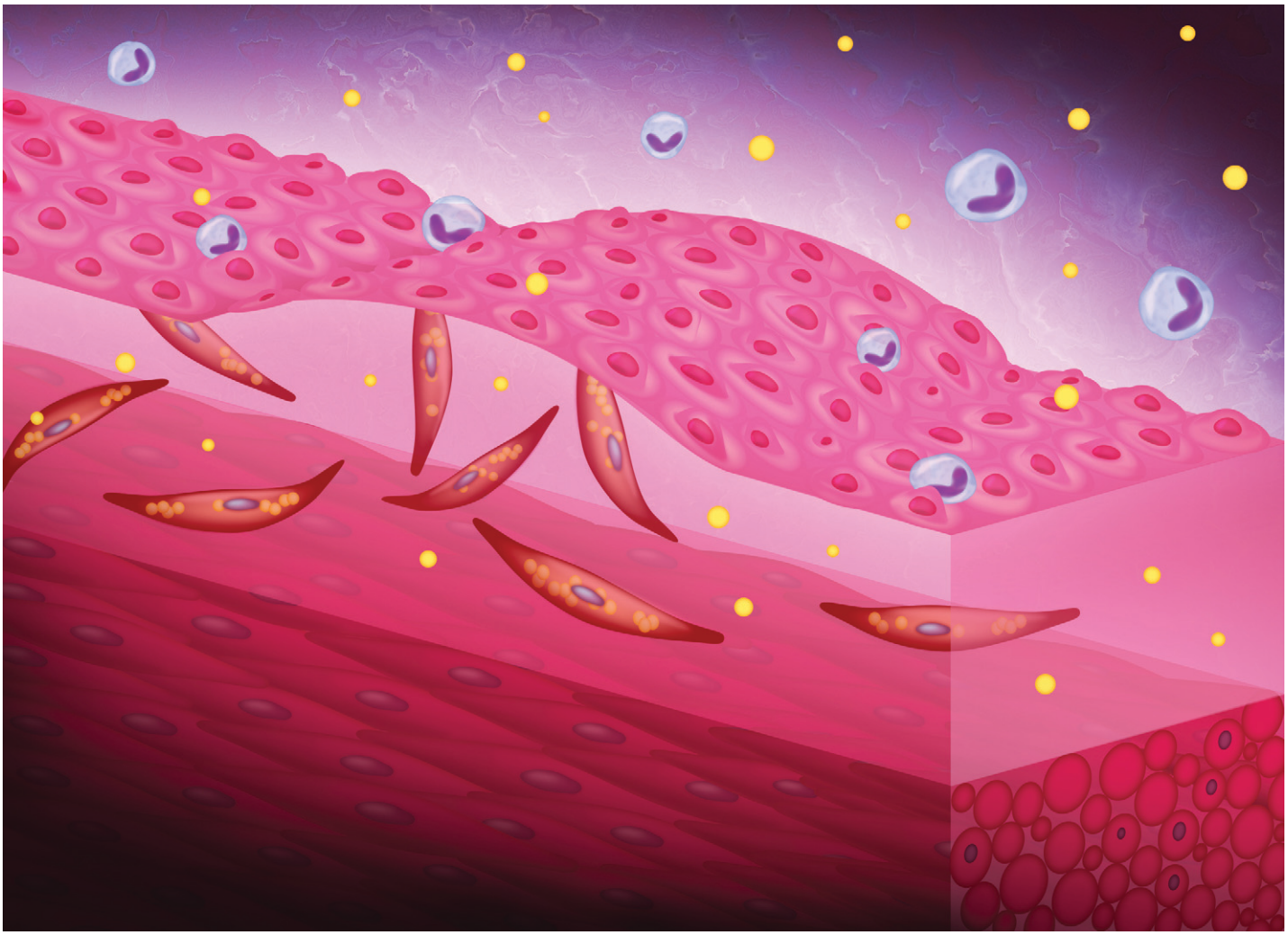

Featuring work from BioMicroSystems Laboratory led by Assistant Professor Han Wei Hou, School of Mechanical and Aerospace Engineering and Lee Kong Chian School of Medicine, Nanyang Technological University, Singapore.

A novel human arterial wall-on-a-chip to study endothelial inflammation and vascular smooth muscle cell migration in early atherosclerosis

A novel arterial wall-on-a-chip with well-defined intima-media structure was developed to model early atherosclerosis. The 3D model recapitulated the contractile and quiescent state of human vascular smooth muscle cells by co-culturing with endothelial cells in compartmentalized extracellular matrix layers. Upon atherogenic stimulation, the model exhibited various phenotypic changes including smooth muscle cell migration, cellular uptake of lipoprotein, and monocyte adhesion. The model can be used to study cellular crosstalk in atherosclerosis and evaluate the atheroprotective efficacy of drug candidates on vascular dysfunction.

As featured in:

See Han Wei Hou *et al.*, *Lab Chip*, 2021, **21**, 2359.

ROYAL SOCIETY OF CHEMISTRY

rsc.li/loc

Registered charity number: 207890

Lab on a Chip

PAPER

View Article Online
View Journal | View Issue

Cite this: *Lab Chip*, 2021, **21**, 2359

A novel human arterial wall-on-a-chip to study endothelial inflammation and vascular smooth muscle cell migration in early atherosclerosis†

Chengxun Su,[ab] Nishanth Venugopal Menon,[a] Xiaohan Xu,[a] Yu Rong Teo,[a] Huan Cao,[c] Rinkoo Dalan,[de] Chor Yong Tay [c] and Han Wei Hou *[ad]

Received 20th February 2021,
Accepted 4th May 2021

DOI: 10.1039/d1lc00131k

rsc.li/loc

Mechanistic understanding of atherosclerosis is largely hampered by the lack of a suitable *in vitro* human arterial model that recapitulates the arterial wall structure, and the interplay between different cell types and the surrounding extracellular matrix (ECM). This work introduces a novel microfluidic endothelial cell (EC)–smooth muscle cell (SMC) 3D co-culture platform that replicates the structural and biological aspects of the human arterial wall for modeling early atherosclerosis. Using a modified surface tension-based ECM patterning method, we established a well-defined intima–media-like structure, and identified an ECM composition (collagen I and Matrigel mixture) that retains the SMCs in a quiescent and aligned state, characteristic of a healthy artery. Endothelial stimulation with cytokines (IL-1β and TNFα) and oxidized low-density lipoprotein (oxLDL) was performed on-chip to study various early atherogenic events including endothelial inflammation (ICAM-1 expression), EC/SMC oxLDL uptake, SMC migration, and monocyte–EC adhesion. As a proof-of-concept for drug screening applications, we demonstrated the atheroprotective effects of vitamin D ($1,25(OH)_2D_3$) and metformin in mitigating cytokine-induced monocyte–EC adhesion and SMC migration. Overall, the developed arterial wall model facilitates quantitative and multi-factorial studies of EC and SMC phenotype in an atherogenic environment, and can be readily used as a platform technology to reconstitute multi-layered ECM tissue biointerfaces.

Introduction

Cardiovascular diseases (CVDs) are the leading causes of death worldwide, with an estimated 31% (17.9 million) of all global death in 2016.[1] The main pathological cause of CVD is atherosclerosis, which is the formation of fibrofatty plaque in the intima that can result in plaque ruptures and thrombosis, causing acute myocardial infarctions, stroke and heart failure.[2,3] Atherosclerosis manifests as a result of the complex interplay between circulating factors, endothelial cells (ECs), vascular smooth muscle cells (SMCs), blood cells and aberrated hemodynamics. Hypertension, hyperlipidemia or hyperglycemia causes endothelial activation through increased oxidative stress, which results in accumulation and oxidation of low-density lipoprotein (LDL) in the subendothelial extracellular matrix (ECM). This will initiate endothelial inflammation, followed by leukocyte recruitment and foam cell formation. Meanwhile, SMCs, the most abundant cells in the tunica media, undergo phenotypic switching from a quiescent/contractile state to a de-differentiated/synthetic state, leading to over-proliferation and migration into the intima that furthers plaque growth.[3] Assessment of biochemical factors modulating the SMC phenotype is thus highly useful for gaining insights into the pathogenesis of atherosclerosis.

Animal models have been widely used for studying changes in SMCs in atherosclerosis, but the experimental process is costly and laborious, and the translation to humans is difficult owing to the interspecies differences in key disease pathways.[4,5] Conventional *in vitro* arterial wall models are mostly based on well plates[6] and transwells[7] with human EC–SMC co-culture. These have limited predictability for *in vivo* tissue functions due to the poor physiological correlation with the *in vivo* situation. In tissue engineering, co-culture of ECs and SMCs in tubular bioreactors,[8,9] or on micropatterned surfaces[10,11] has been reported, but is limited

[a] *School of Mechanical and Aerospace Engineering, Nanyang Technological University, Singapore, 639798, Singapore. E-mail: hwhou@ntu.edu.sg*
[b] *Interdisciplinary Graduate School, Nanyang Technological University, Singapore, 639798, Singapore*
[c] *School of Materials Science & Engineering, Nanyang Technological University, Singapore, 639798, Singapore*
[d] *Lee Kong Chian School of Medicine, Nanyang Technological University, Singapore, 308232, Singapore*
[e] *Endocrinology Department, Tan Tock Seng Hospital, Singapore, 308433, Singapore*

† Electronic supplementary information (ESI) available. See DOI: 10.1039/d1lc00131k

by complex fabrication and lack of study on SMC phenotypic modulation. Microfluidic organ-on-chip (or microphysiological systems) technology is an exciting new form of cell-based *in vitro* model which enables precise control of the 3D microenvironment and spatial distribution of different tissue layers to replicate key aspects of human organs.[12] A microfluidic arterial wall model was reported using ECs and SMCs cultured as 2D monolayers on a porous membrane with biomechanical cues.[13] Other microfluidic artery models have integrated the ECM into microfluidic devices for 3D culture of SMCs and ECs in two separate chambers of collagen,[14] or 3D culture of SMCs in collagen adjacent to an EC-lined lumen.[15–17] However, these models mostly focus on vascular geometries or endothelial functions with little emphasis on establishing important SMC characteristics including the well-defined laminar structure and quiescent SMC phenotype. These severely limit their applications to study SMC phenotypic modulation in atherosclerosis. Hence, there exists a critical need to develop novel *in vitro* EC–SMC co-culture models with a focus on recreating artery-like SMC architecture, and enabling the study of SMC phenotypic modulation in response to environmental cues.

Herein, we introduce a novel microfluidic 3D "arterial wall-on-a-chip" that has a morphologically distinct EC–SMC co-culture, and recapitulates the arterial intima–media interface through precise control of the ECM microenvironment using collagen and a basement membrane matrix (Matrigel). Two lanes of hydrogel, one serving as the subendothelial ECM layer and the other for SMC 3D culture, were sequentially patterned in the device using a modified surface tension-based hydrogel confinement method. By fabricating a three-layered PDMS device with two channel stepped heights, hydrogel can be sequentially confined within the shallower channel based on the capillary burst valve effect,[15] thus enabling dual hydrogel lanes to form without any physical barrier in between. We first characterized the ECM composition in the subendothelial layer, and observed that high Matrigel content (collagen 20%, Matrigel 80%) could retain the SMCs in a quiescent state for up to a week. Comparative studies were performed to study the crosstalk between ECs and SMCs, and the effect of the subendothelial ECM on the morphogenesis of SMCs. As a disease model for atherosclerosis, the responses of ECs and SMCs to pro-inflammatory cytokines (IL-1β, TNFα) and oxidized LDL (oxLDL) were investigated. Besides endothelial inflammation, significant SMC phenotypic changes were observed with increased oxLDL uptake and migration towards the intima during hyperlipidemia. Lastly, we studied the protective effects of vitamin D (1*A*,25-dihydroxyvitamin D3) and metformin in atherosclerosis,[18,19] and showed that they can mitigate monocyte–EC adhesion (using THP-1 cells) and SMC migration in a cytokine-induced inflamed vascular model. Taken together, the developed microfluidic model is the first-in-kind platform which facilitates quantitative and real-time studies of EC–SMC interactions and SMC phenotypic modulation in an atherogenic environment, and can be further developed to incorporate biomechanical cues (shear flow) or immune components for multi-factorial vascular drug screening.

Experimental section

Device fabrication

A three-step photolithography was performed to fabricate a mold with two stepped heights required for the pillar-free two-lane hydrogel confinement. Standard soft lithography was used to fabricate the microdevice. In brief, the polydimethylsiloxane (PDMS) prepolymer was mixed with the curing agent (Dow Corning) in a ratio of 10 : 1 (w/w) and poured over the patterned silicon wafer, degassed and cured for 2 hours at 75 °C. The replica molded PDMS slab was then cut and peeled off from the wafer carefully. A biopsy puncher (1.5 mm) was used to create the inlet and outlet for the device and the PDMS slab was bonded to a glass slide or cover slip by plasma bonding (Harrick Plasma cleaner). The bonded device was kept at 75 °C for 24 hours to allow for hydrophobic recovery and sterilized by ultraviolet light for 30 min prior to any on-chip cell culture experiments.

Characterization of the hydrogel confinement

Collagen type I (rat tail, Corning, 3 mg ml^{-1}) was prepared as previously described by Shin *et al.*[20] Collagen with fluorescein isothiocyanate (FITC)-dextran 70 kDa (Sigma, 1 μM) was loaded into the first hydrogel channel (designated as the subendothelial ECM channel), followed by 30 min of incubation at 37 °C to allow for polymerization. Next, collagen with rhodamine 6G (Sigma, 1 μM) was loaded into the second hydrogel channel (designated as the SMC 3D culture channel). The device was imaged using a fluorescence microscope (Nikon Eclipse Ti).

Cell culture

Primary human aortic endothelial cells (ECs) were gifted by Prof Lena Ho (Duke NUS), and primary human aortic smooth muscle cells (SMCs) were obtained from a commercial supplier (Lonza). ECs were maintained using endothelial cell growth medium-2 (EGM-2) BulletKit (Lonza) supplemented with 1% penicillin–streptomycin (P/S), and SMCs were maintained using smooth muscle cell growth medium-2 (SmGM-2) BulletKit (Lonza) supplemented with 1% P/S. The cells were expanded in T75 flasks and maintained at 37 °C in a humidified 5% CO_2 incubator and passaged at 70–80% confluency using 0.25% trypsin with 1 mM EDTA (Gibco). Passage numbers 3 to 10 were used for ECs, and passage numbers 6 to 10 were used for SMCs. For on-chip culture, serum-depleted SmGM-2 supplemented with insulin–transferrin–selenium premix (Corning) was used. THP-1 human monocytic leukemia cells (ATCC® TIB-202™) were maintained in RPMI-1640 medium (Gibco) supplemented with 10% fetal bovine serum (Gibco) and 1% P/S.

On-chip culture of ECs and SMCs

First, 3 mg ml^{-1} collagen type I (rat tail, Corning) was prepared as previously described,[20] and a frozen aliquot of Matrigel (10 mg ml^{-1}, Corning) was thawed on ice. Then, a gel mixture of collagen and Matrigel (volumetric ratio of 1 : 4) was prepared and maintained on ice. For each device, the gel mixture (~15 μl) was loaded into the subendothelial ECM channel by pipetting and allowed to polymerize for 30 min at 37 °C. Meanwhile, SMCs were dissociated and resuspended into 3 mg ml^{-1} collagen I at a concentration of 1 million cells per ml. The SMC-laden collagen was loaded into the SMC culture channel and allowed to polymerize for 30 min at 37 °C, following which serum depleted SmGM-2 was loaded into the SMC medium channel to replenish the cells. In the meantime, the EC channel was coated with 0.5 mg ml^{-1} polydopamine solution for 30 min at 37 °C to facilitate cell adhesion. The polydopamine solution was prepared by dissolving dopamine hydrochloride (Sigma) in Tris–HCl buffer, pH 8.5. The EC channel was subsequently washed with 1× phosphate buffered saline (PBS) 3 times before cell seeding. Lastly, ECs were trypsinized and resuspended in EGM-2 to a concentration of 4 million cells per ml and loaded into the EC channel. The device was then incubated for 45 min at 37 °C to allow for EC adhesion, and droplets of EGM-2 and SmGM-2 (35 μl each) were placed at the inlet and outlet of the respective channel. The device was incubated at 37 °C in humidified 5% CO_2 for 3 days with daily change of medium until the ECs reach confluency and SMCs fully aligned. For SMC monoculture, the EC channel was not seeded with cells, but loaded with EGM-2 medium. For EC–SMC co-culture without a subendothelial layer, the SMC gel was loaded into the subendothelial channel, following which the SMC culture channel and SMC medium channel were both loaded with serum depleted SmGM-2 medium, while the EC channel was seeded with ECs as described above.

ECM optimization for the subendothelial layer

For investigating the optimal ECM material for the subendothelial layer, collagen (3 mg ml^{-1}) and Matrigel (10 mg ml^{-1}) were mixed on ice at volumetric ratios of 1 : 4, 1 : 1, and 4 : 1 as indicated in Table 1, yielding three gel mixtures C2M8, C5M5 and C8M2, respectively.

For gel elasticity measurement, collagen I (3 mg ml^{-1}) and gel mixtures C2M8, C5M5, C8M2 were prepared and deposited into PDMS wells created using a 1.5 mm biopsy puncher (each well ~300 μL of gel). The gels were incubated at 37 °C, 5% CO_2 for 30 min, and immersed in EGM-2 medium for 1 day prior to measurement. The storage modulus of the gels at 0.5% strain, 0.5 Hz was recorded using a rheometer (Anton Parr MCR501).

Table 1 ECM composition for C2M8, C5M5, and C8M2

Gel mixture	Composition	
	Collagen I% (volumetric)	Matrigel% (volumetric)
C2M8	20%	80%
C5M5	50%	50%
C8M2	80%	20%

Immunostaining

The EC channel and SMC medium channel were washed 3 times with 1× PBS, and fixed with 4% paraformaldehyde (Sigma) for 15 min. Fixed cells were permeabilized with 0.1% Triton-X 100 in PBS for 15 min, washed 3 times with 1× PBS, and blocked with 0.5% bovine serum albumin (BSA) in PBS for 2 hours at room temperature. The EC channel was loaded with VE-cadherin rabbit anti-human CD144 primary antibody (10 μg ml^{-1}, Enzo) for immunolabeling of ECs, while the SMC medium channel was loaded with MYH11 antibody (G-4) Alexa Fluor® 647 (20 μg ml^{-1}, sc-6956 AF647, Santa Cruz) and calponin 1 antibody (CALP) Alexa Fluor® 488 (20 μg ml^{-1}, sc-58707 AF488, Santa Cruz) for immunolabeling of SMCs. The cells were then incubated overnight at 4 °C. Subsequently, the cells were rinsed with 0.1% BSA in PBS 3 times, and ECs were fluorescently labeled with AlexaFluor 488 goat anti-rabbit secondary antibody (20 μg ml^{-1}, Life Technologies) for 4 hours at room temperature. Lastly, both ECs and SMCs were labeled for F-actin and cell nuclei with AlexaFluor 568 phalloidin (0.17 μM, Life Technologies) and Hoechst 33342 (1 μg ml^{-1}, Life Technologies), respectively, by incubating at room temperature for 45 min. For inflammation and hyperlipidemia studies, the chips were fixed and stained for ICAM-1 and nuclei with FITC-labeled anti-human CD54 (5 μg ml^{-1}, Biolegend) and Hoechst 33342, respectively, for 45 min at room temperature. The cells were imaged using a fluorescence microscope (Nikon Eclipse Ti) or a confocal microscope (Carl Zeiss LSM 800, Germany).

Inflammation, hyperlipidemia, vitamin D and metformin studies

To induce inflammation, tumor necrosis factor alpha (TNFα, Peprotech) and/or interleukin-1 beta (IL-1β, Sigma) were added to EGM-2 medium at 1 ng ml^{-1} and loaded into the EC channel at day 3. The devices were then incubated at 37 °C for 48 hours without medium change. For hyperlipidemia treatment, low density lipoprotein from human plasma, oxidized DiI conjugate (DiI-oxLDL, Sigma) was added into EGM-2 (with or without TNFα (1 ng ml^{-1}) and IL-1β (1 ng ml^{-1})) at 10 μg ml^{-1} or 50 μg ml^{-1}. For vitamin D studies, 1*A*,25-dihydroxyvitamin D3 (Sigma) was added into EGM-2 with TNFα (1 ng ml^{-1}) and IL-1β (1 ng ml^{-1}) at 20 nM or 100 nM. For metformin studies, 1,1-dimethylbiguanide hydrochloride (MedChemExpress) was added into EGM-2 with TNFα (1 ng ml^{-1}) and IL-1β (1 ng ml^{-1}) at 2 mM or 20 mM. For quantification of EC inflammation and Dil-oxLDL uptake, the fluorescence intensities of ICAM-1 and Dil-oxLDL were calculated using eqn (1):

$$I = (I_t - I_b)/n \quad (1)$$

where I_t is the integrated intensity, I_b is the background intensity, and n is the number of cells. We estimated I_b by measuring the mean gray value of regions without cells and multiplying this value to the area of the image. The intensity of ICAM-1 was expressed as fold change after normalizing to the untreated chip of each batch, whereas the intensity of Dil-oxLDL was normalized to the chip treated with Dil-oxLDL 10 μg ml^{-1} of each batch.

Image analysis for SMCs

To quantify the migration of SMCs, chips were fixed and stained at day 3 for subendothelial ECM composition studies, and at day 5 for inflammation and hyperlipidemia studies. The migrated cells (present in the subendothelial ECM) were counted using ImageJ (NIH). The migration distance of individual cells was measured by drawing a perpendicular line from the nuclei of migrated SMCs to the upper border of the SMC layer. For quantification of the aspect ratio and angle orientation of the SMCs (non-migrated), the boundary of the cells was drawn according to the F-actin and nuclei staining on ImageJ. The cell shape was approximated to an ellipse, following which the angle orientation and length of the major and minor axis were measured. All angles were normalized to be between 0° and 90°. The aspect ratio of SMCs was expressed as the ratio of the major and minor axis. Eqn (1) was used for quantification of calponin 1 intensity and MYH11 intensity.

On-chip monocyte adhesion assay

Monocytic THP-1 cells were resuspended in EGM-2 and loaded into the EC channel at a concentration of 2.5 million cells per ml and incubated for 1 hour at 37 °C. After incubation, the channels were washed three times to remove unbound cells before imaging with an inverted phase-contrast microscope (Nikon Eclipse Ti). Adhered THP-1 cells were quantified using ImageJ.

Statistical analysis

Data were analyzed with unpaired Student's *t*-test or one-way ANOVA with Tukey's multiple comparison test (GraphPad). Differences between groups were considered statistically significant when $p < 0.05$. Results in the form of bar graphs were presented as mean ± standard deviation (SD). Results in the form of a scatter plot were indicated with a line at the mean. All data points were derived from three or more replicates, as indicated in the caption for each figure.

Results

Microengineered arterial wall-on-a-chip recapitulated the arterial intima–media interface

The human arterial wall is composed of three layers: 1) the innermost layer intima is lined with ECs which reside on a layer of subendothelial ECM that provides mechanical strength while allowing nutrient diffusion, 2) the media consists of layers of quiescent SMCs embedded in a well-organized ECM, and 3) the outermost adventitia provides protection to the inner layers. During atherosclerosis, the SMC undergoes phenotypic switching to a proliferative and migratory state, which contributes to significant ECM remodeling and intima thickening (Fig. 1A). Our microfluidic device consists of four parallel straight channels, and the dimensions were designed to reconstitute the atherogenic arterial intima–media interface which comprises a thicker subendothelial layer due to intima thickening in atherosclerosis. The first fluidic channel was for EC culture, followed by a "cell-free" hydrogel channel serving as the subendothelial ECM layer. An adjacent hydrogel channel was designed for 3D culture of SMCs, further to which was a fluidic channel that provided culture medium for SMCs. Each cell type was cultured with its own medium while still in constant diffusive contact. ECM patterning was based on the capillary burst valve (CBV) effect generated due to changes in channel heights (Fig. 1B). In brief, the subendothelial ECM channel (the shallowest channel, 100 μm in height) was loaded with the first hydrogel (green), and was well confined by the CBV effect without overflowing to the adjacent channel due to the increase of channel height at both sides. After gelation, the second hydrogel (red) was loaded and confined in the adjacent SMC culture channel (125 μm in height) with the first cross-linked hydrogel acting as a "solid" side wall (Fig. 1B and C). To achieve robust gel confinement by manual pipetting, the channel widths are set as ~600 μm to 800 μm. A smaller channel width (~400 μm) is also possible but requires careful pipetting and pressure control to avoid overflow of gel into the adjacent channel (Fig. S1†). For the arterial wall-on-a-chip, the channel width for the subendothelial layer was determined to be 600 μm which is comparable to the intima thickness of an adult human coronary artery (averaged at ~0.4 mm for a non-atherosclerotic artery, and up to ~1 mm at atheroma sites).[21–24] The channel width for the SMC layer was kept constant at 600 μm, which is also within the range of the intima/media thickness ratio in an adult human coronary artery (~0.4–3).[24,25]

SMC phenotype altered by the ECM composition of the subendothelial layer

In the EC–SMC co-culture, Matrigel (10 mg ml^{-1}), a basement membrane-derived matrix,[26] was initially used as the subendothelial ECM layer to function as the basement membrane layer underneath the endothelium, whereas collagen type I (3 mg ml^{-1}), an abundant ECM component in the tunica media,[27–29] was used for 3D culture of SMCs. However, significant gel contraction of the SMC layer was observed at the boundary against Matrigel (data not shown). Therefore, gel mixtures of Matrigel and collagen, namely C2M8 (80% Matrigel), C5M5 (50% Matrigel), C8M2 (20% Matrigel), were investigated for use as subendothelial ECMs (Table 1). Consequently, gel contraction of the SMC layer was not observed for all the 3 aforementioned gel mixtures, suggesting that the collagen in the mixtures played an important role in

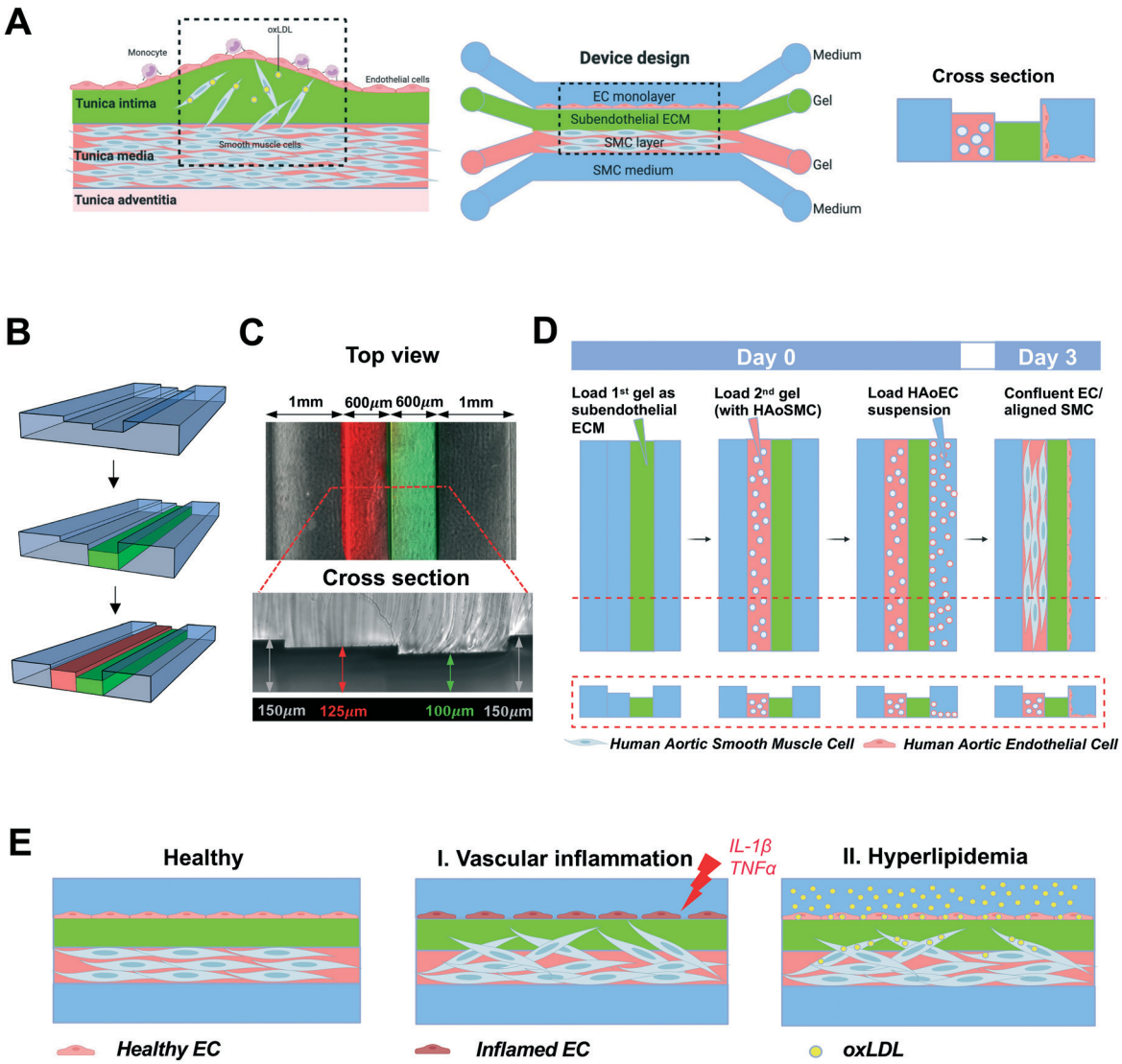

Fig. 1 Microengineered arterial wall-on-a-chip device. (A) Schematic illustration of EC/SMC dysfunction in the arterial wall in early atherosclerosis (left). Schematic of microfluidic design (top view) (middle). Black dotted box indicates the region of the intima–media interface modeled using the device. Schematic of microfluidic design (cross-sectional view) (right). (B) Exploded view of the pillar-free two-lane hydrogel patterning based on the CBV effect. Green hydrogel indicates the subendothelial ECM layer; red hydrogel indicates the SMC layer. (C) Brightfield overlaid with a fluorescence image (top view) of the device after gel loading (green – first hydrogel (subendothelial ECM layer); red – second hydrogel (SMC layer)). Red dotted line indicates the channel cross-sectional view. (D) Protocol for ECM loading and co-culture of ECs and SMCs in the device. Red dotted line indicates the channel cross-sectional view. (E) Schematic of the changes in SMC phenotype under different atherogenic conditions (vascular inflammation and hyperlipidemia).

anchoring the SMC-laden collagen to the subendothelial layer. Interestingly, most SMCs remained in the SMC layer when C2M8 was used as the subendothelial layer, and there was substantial migration of SMCs into the intima for C5M5 and C8M2 (Fig. 2A). Quantification of the migrated cell number and distance confirmed this observation, marked by a 3.8-fold increase in migrated cell number (12.75 ± 5.12 (C2M8) *vs.* 48.00 ± 9.66 (C8M2), $p < 0.001$), and a concomitant increase in mean migration distance by 3-fold (89.32 μm (C2M8) *vs.* 279.5 μm (C8M2), $p < 0.0001$) (Fig. 2B).

Another striking difference resulting from the varying subendothelial Matrigel content was the SMC morphology. The SMCs residing adjacent to C2M8 exhibited a spindle-shaped and aligned morphology (Fig. 2A and C), resembling the quiescent state SMCs in healthy arteries.[3,28] In contrast, the SMCs exhibited a rhomboidal and less polarized cell shape (Fig. 2A and C) for the subendothelial ECM with lower Matrigel content, which was consistent with the cell morphology commonly associated with SMC activation during vessel repair or in atherosclerosis.[30,31] The cell shape and angle orientation of the non-migrated SMCs were quantified and corroborated the spindle shape of SMCs residing adjacent to C2M8 (mean aspect ratio: 9.1) (Fig. 2D and E), and the parallel alignment along the length of endothelium (>72% cells distributed within 0–10°) (Fig. 2F). Besides the difference in cell migration and

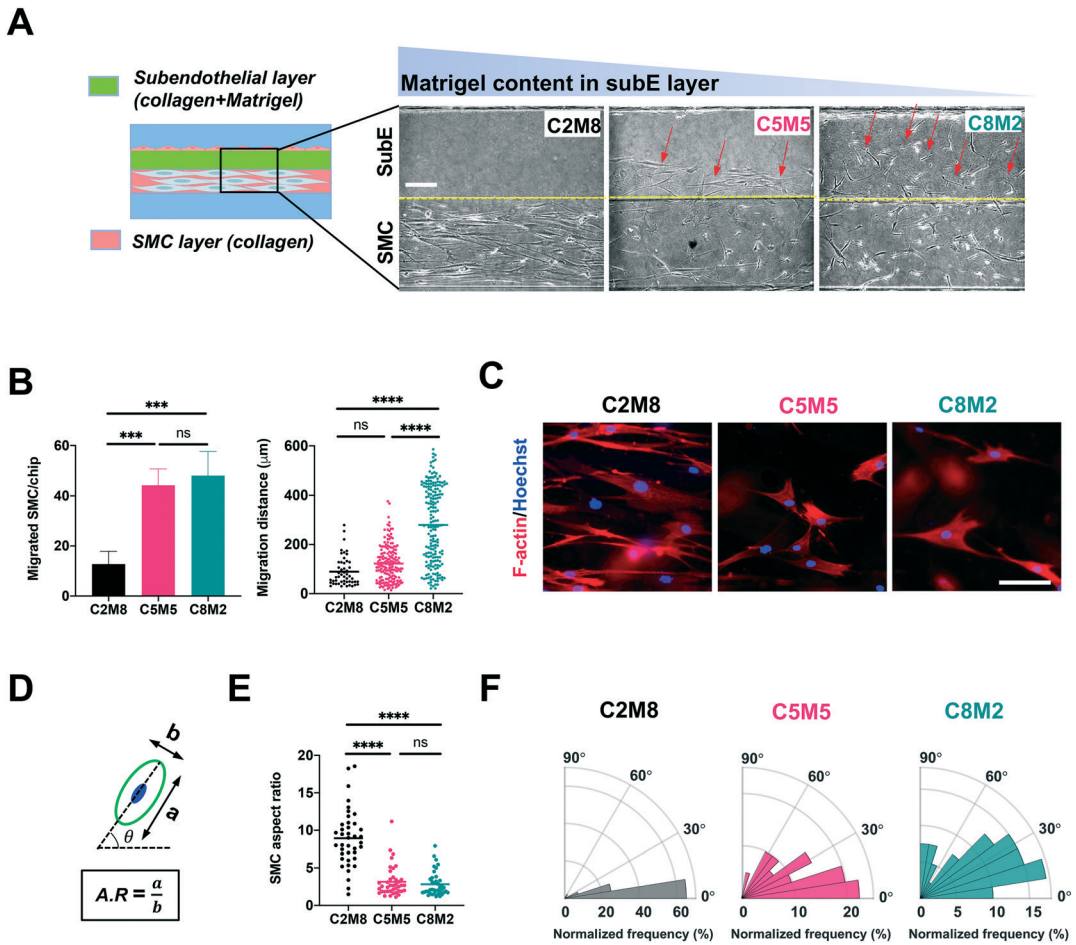

Fig. 2 SMC phenotype altered by the ECM composition of the subendothelial layer. (A) Brightfield images of the subendothelial (subE) layer and SMC layer region with different subendothelial ECM compositions (C2M8, C5M5, C8M2) at day 3 of EC–SMC co-culture. Yellow dotted line indicates the boundary between layers; red arrow indicates migrated SMCs. Scale bar: 200 μm. (B) Quantification of SMC migration into the subendothelial layer in terms of cell count (left) and migration distance (right) (n = 4 chips from 4 independent experiments). Results were expressed as mean ± SD for migrated SMC/chip, or as a scatter plot with a line at the mean for the migration distance. Data were analyzed with one-way ANOVA with Tukey's multiple comparison test (****$p < 0.0001$, ***$p < 0.001$, "ns" – not significant). (C) Fluorescence images of non-migrated SMCs within the SMC layer showing different morphologies (red – F-actin, blue – nuclei). Scale bar: 100 μm. (D) Schematic of the aspect ratio and angle orientation of SMCs. (E) Aspect ratio of non-migrated SMCs (~40–50 cell measurements from n = 4 chips from 4 independent experiments). Results were expressed as a scatter plot with a line at the mean. Data were analyzed with one-way ANOVA with Tukey's multiple comparison test. (F) Angle orientation distribution of non-migrated SMCs (~40–50 cell measurements from n = 4 chips from 4 independent experiments).

morphology, we also showed a decreased expression level of contractile markers (calponin 1 and smooth muscle myosin heavy chain 11 (MYH11)) for SMCs cultured under C8M2 conditions (Fig. S2†). Collectively, it was evident that high Matrigel content in the subendothelial layer gave rise to a contractile and quiescent-state SMC phenotype, suggesting the importance of the subendothelial basement membrane in maintaining the artery physiology. Therefore, the gel mixture C2M8 was determined as the most optimal material for the subendothelial ECM layer, owing to its attribute of anchoring the intima to the media layer efficiently while allowing the SMCs to remain non-migratory, spindle-shaped and aligned, similar to what was observed *in vivo*.[28,29,32,33]

As the cellular phenotype can be affected by the elasticity of the ECM,[34–36] we further characterized the mechanical properties of the three subendothelial gel mixtures using a rheometer. There were no significant differences in storage modulus among the three gel mixtures, although the value for C2M8 was around twice that of pure collagen (95.2 ± 19.72 Pa (C2M8) *vs.* 48.2 ± 8.83 Pa (collagen), $p < 0.01$) (Fig. S3†). While further studies are warranted, this suggested that the quiescent SMC observed here was likely due to the biochemical cues presented by the basement membrane matrix (Matrigel), which is consistent with the previously reported role of laminin and collagen IV in maintaining the SMC contractile phenotype *in vitro*.[37–40]

EC–SMC co-culture with a cell-free subendothelial ECM layer promoted SMC quiescent phenotype

To study EC–SMC cellular interactions, a comparative study between EC–SMC co-culture and SMC monoculture was

performed using the developed model. In the absence of ECs, the SMCs became significantly more migratory (Fig. 3A), as evidenced by a 5.7-fold increase in migrated cell number and a 2.6-fold increase in migration distance (Fig. 3B). Morphologically, the monocultured SMCs (non-migrated) retained the spindle shape, but appeared less elongated and aligned as compared to co-culture (Fig. 3A, B and S4†). These indicated the critical role of ECs in retaining a quiescent SMC phenotype, as reported by previous studies.[6,41,42] Next, we investigated if the absence of a subendothelial layer affected the co-culture. Evidently, a substantial amount of SMCs migrated into the EC channel when there was no subendothelial layer in between, which almost fully disrupted the formation of an intact EC barrier along the ECM side wall (Fig. S5†). Moreover, SMCs (both migrated or non-migrated) appeared either atrophic or remained rounded, suggesting that the biochemical cues presented by the subendothelial ECM were essential for SMC survival and growth. Confocal imaging was then performed for the co-cultured cells on the chip, which showed a 3D SMC bundle consisting of dense layers of well-aligned cells. The actin filament in the SMC also organized into aligned microfibrils (Fig. 3C). The

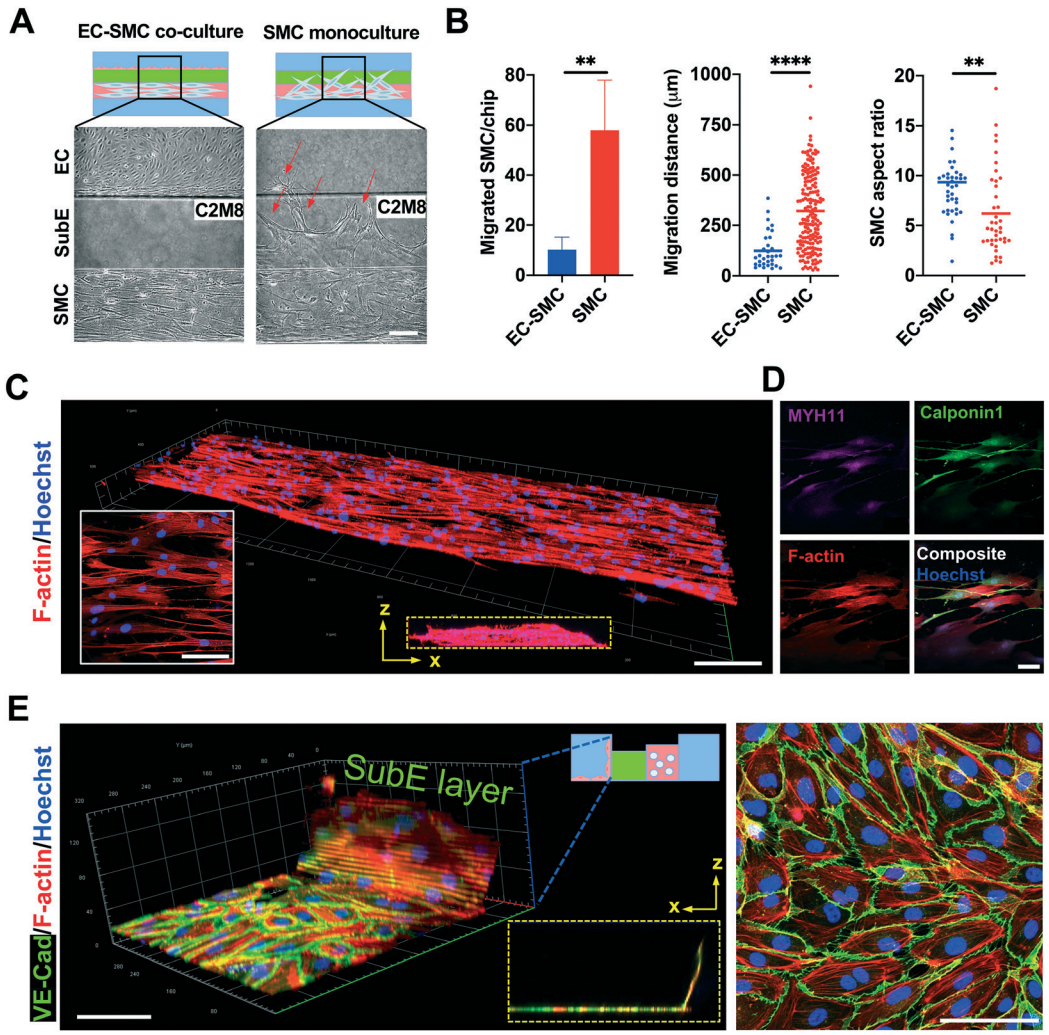

Fig. 3 Characterization of SMC phenotype under EC–SMC co-culture and SMC monoculture. (A) Brightfield images of co-culture and monoculture (C2M8 as the subendothelial layer) at day 3. Red arrow indicates migrated SMCs. Scale bar: 200 μm. (B) Quantification of SMC migration into the subendothelial layer in terms of cell count (left) and migration distance (middle). Aspect ratio of non-migrated SMCs (right) (n = 3–4 chips from 3 independent experiments for migration studies, ~40–50 cell measurements from n = 3 chips from 3 independent experiments for the aspect ratio). Results were expressed as mean ± SD for migrated SMC/chip, or as a scatter plot with a line at the mean for the SMC migration distance and aspect ratio. Data were analyzed with unpaired Student's t-test (****$p < 0.0001$, **$p < 0.01$). (C) 3D reconstructed fluorescence image of SMCs co-cultured with ECs (red – F-actin, blue – nuclei). Image inset (white box) shows a magnified view illustrating co-alignment of actin filament. Image inset (yellow dotted box) indicates the z-stack projection (maximum intensity) of transversal confocal sections. Scale bar: 100 μm. (D) Fluorescence image of co-cultured SMCs (magenta – MYH11, green – calponin 1, red – F-actin, blue – nuclei). Scale bar: 50 μm. (E) 3D reconstructed fluorescence image of ECs on the channel surface and along the subendothelial layer (green – VE-Cad, red – F-actin, blue – nuclei). Image inset (yellow dotted box) indicates the z-stack projection of transversal confocal sections of ECs. Magnified fluorescence image of the EC monolayer on the channel surface (right). Scale bar: 100 μm.

contractile state of the SMC was validated by positive immunostaining of contractile makers calponin 1 and MYH11 (Fig. 3D). As expected, the ECs formed a confluent monolayer along the *Z* direction (residing on the subendothelial layer), which contained continuous adherens junctions between adjacent cells as indicated by vascular endothelial cadherin (VE-Cad) staining (Fig. 3E).

IL-1β and TNFα-induced vascular inflammation elevated SMC migration

As pro-inflammatory cytokines such as IL-1β and TNFα are key mediators in the inflammation cascade in atherosclerosis,[43,44] we investigated the cellular responses to IL-1β and TNFα using the developed model by adding the cytokines to the EC medium (Fig. 4A). Interestingly, SMCs began to migrate towards the intima after 48 hours of treatment with IL-1β (1 ng ml^{-1}), TNFα (1 ng ml^{-1}), or IL-1β (1 ng ml^{-1}) plus TNFα (1 ng ml^{-1}), indicative of SMC phenotypic modulation (Fig. 4B). Endothelial inflammation was also confirmed based on upregulation of intercellular adhesion molecule 1 (ICAM-1) in ECs (Fig. 4C). SMC migration was significantly increased when the EC was co-treated with IL-1β and TNFα, marked by a 3.6-fold increase in migrated cell number (8.75 ± 2.36 (untreated) *vs.* 31.5 ± 2.65 (IL-1β+ TNFα), $p < 0.0001$), and a 1.8-fold increase in mean migration distance (95.22 μm (untreated) *vs.* 171 μm (IL-1β+ TNFα), $p < 0.01$) (Fig. 4D). These results suggested a cumulative effect of IL-1β and TNFα in modulating the SMC migration. As inflammatory cytokines could compromise the EC barrier integrity[45,46] to allow cytokine diffusion through the subendothelial layer to act directly on the SMC, we next

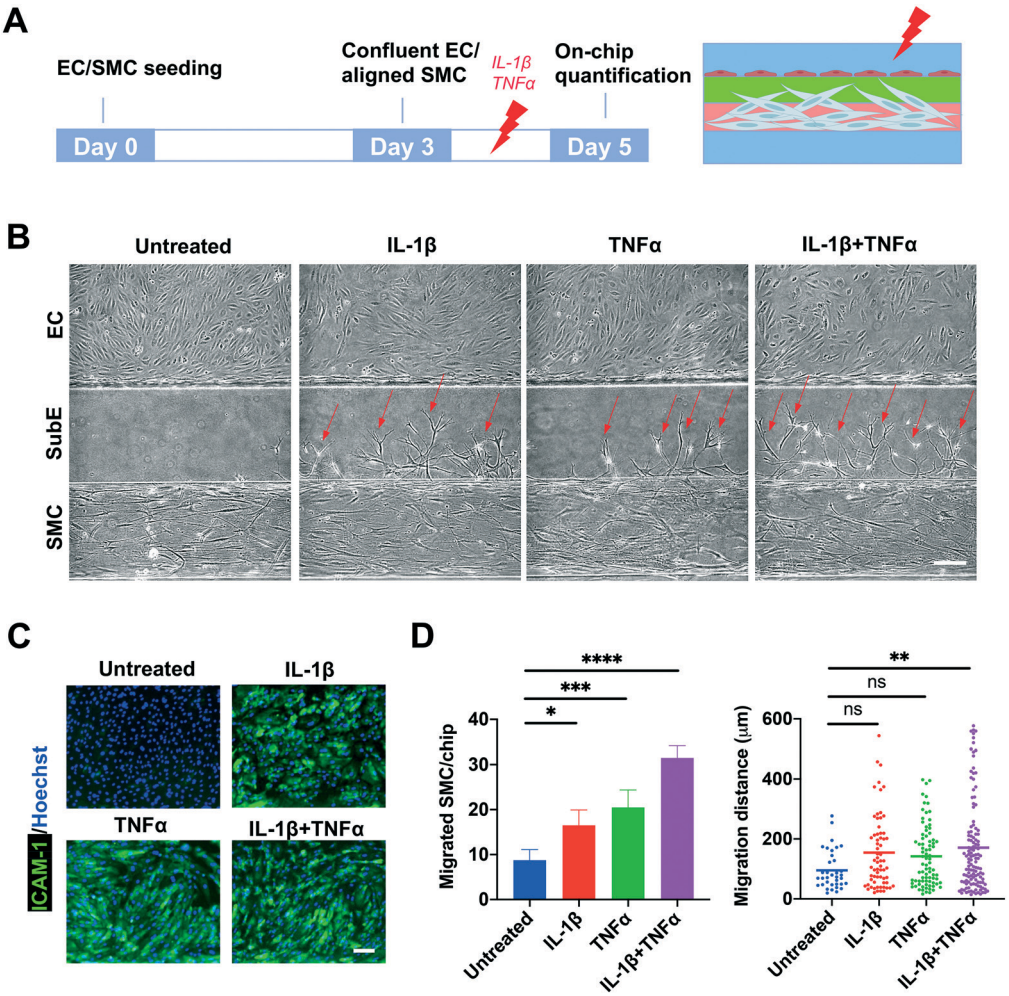

Fig. 4 IL-1β and TNFα-induced vascular inflammation elevated SMC migration. (A) Experimental timeline for inflammatory cytokine treatment (left). Schematic of the chip after cytokine treatment (right). (B) Brightfield image of untreated, IL-1β (1 ng ml^{-1}) treated, TNFα (1 ng ml^{-1}) treated, and IL-1β (1 ng ml^{-1}) + TNFα (1 ng ml^{-1}) treated chips at day 5. Red arrows indicate migrated SMCs. Scale bar: 200 μm. (C) Endothelial ICAM-1 expression (green – ICAM-1, blue – nuclei). Scale bar: 200 μm. (D) Quantification of SMC migration into the subendothelial layer in terms of cell count (left) and migration distance (right) (n = 4 chips from 4 independent experiments). Results were expressed as mean ± SD for migrated SMC/chip, or as a scatter plot with a line at the mean for the migration distance. Data were analyzed with one-way ANOVA with Tukey's multiple comparison test (****$p < 0.0001$, ***$p < 0.001$, **$p < 0.01$, *$p < 0.05$, "ns" – not significant).

investigated whether the SMC migration was caused by EC paracrine signaling or the direct effect of cytokines by treating SMC monoculture with cytokines (added into the EC channel). However, there were no observable differences in SMC migration regardless of cytokine treatments due to the highly migratory state of SMCs in the absence of ECs (Fig. S6† and 4B). While further investigation is warranted to elucidate the effects of cytokine and EC-secreted soluble factors in modulating SMC phenotype during inflammation, these results clearly highlighted a critical role of establishing EC–SMC co-culture for SMC migration studies. Taken together, the developed model representative of the arterial intima–media interface enables simultaneous quantification of both EC and SMC phenotype during vascular inflammation, and will be highly useful to model early stage atherogenic processes.

Hyperlipidemic environment triggered SMC migration

Many animal and *in vitro* studies[47–49] have reported that oxLDL played an important role in SMC phenotypic modulation during the onset and progression of atherosclerosis, but modulation of SMC phenotype in a 3D ECM environment or EC co-culture has not yet been demonstrated. Fluorescently labeled oxLDL (Dil-oxLDL) with or without inflammatory cytokines (IL-1β and TNFα) was added to our artery model over 48 hours (in the EC channel) (Fig. 5A), and EC/SMC oxLDL uptake, EC ICAM-1 expression, and SMC migration were examined. As expected, we observed cellular uptake of oxLDL for both ECs and SMCs after 48 hours of treatment, with an increase in SMC migration for higher dose oxLDL (50 μg ml^{-1}) treatment (Fig. 5B and C). While negligible effects on EC ICAM-1 expression were

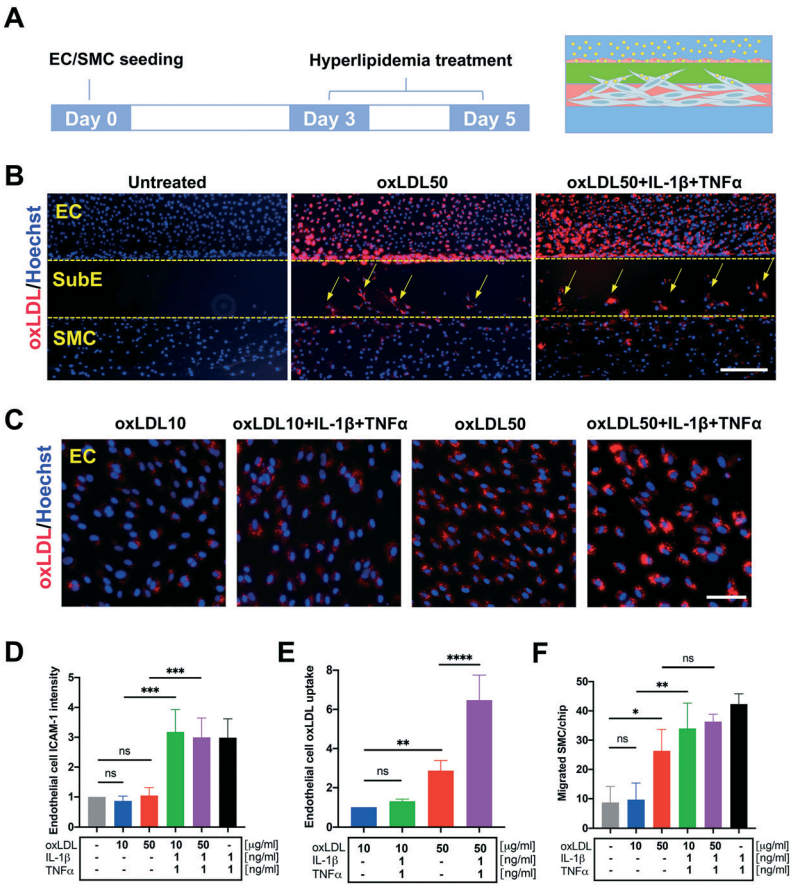

Fig. 5 Hyperlipidemic environment triggered SMC migration. (A) Experimental timeline for hyperlipidemia treatment (left). Schematic of the chip after hyperlipidemia treatment (right). (B) Fluorescence images of untreated, Dil-oxLDL (50 μg ml^{-1}) treated, and Dil-oxLDL (50 μg ml^{-1}) + IL-1β (1 ng ml^{-1}) + TNFα (1 ng ml^{-1}) treated chips at day 5 (red – Dil-oxLDL, blue – nuclei). Yellow dotted lines indicate the layer boundary. Yellow arrows indicate migrated SMCs. Scale bar: 500 μm. (C) Fluorescence images of the EC region for chips treated with Dil-oxLDL (10 μg ml^{-1}), Dil-oxLDL (10 μg ml^{-1}) + IL-1β (1 ng ml^{-1}) + TNFα (1 ng ml^{-1}), Dil-oxLDL (50 μg ml^{-1}), and Dil-oxLDL (50 μg ml^{-1}) + IL-1β (1 ng ml^{-1}) + TNFα (1 ng ml^{-1}), respectively (red – Dil-oxLDL, blue – nuclei). Scale bar: 100 μm. (D) Endothelial ICAM-1 expression (normalized to untreated of each batch) (n = 3–4 chips from 3 independent experiments). Results were expressed as mean ± SD. Data were analyzed with one-way ANOVA with Tukey's multiple comparison test. (E) Endothelial oxLDL uptake (normalized to oxLDL 10 μg ml^{-1} of each batch) (n = 3–4 chips from 3 independent experiments). Results were expressed as mean ± SD. Data were analyzed with one-way ANOVA with Tukey's multiple comparison test. (F) Quantification of SMC migration into the subendothelial layer in terms of cell count (n = 3 chips from 3 independent experiments). Results were expressed as mean ± SD. Data were analyzed with one-way ANOVA with Tukey's multiple comparison test (****$p < 0.0001$, ***$p < 0.001$, **$p < 0.01$, *$p < 0.05$, "ns" – not significant).

elicited by oxLDL alone (Fig. 5D), there was a marked increase in EC oxLDL uptake at 50 μg ml^{-1} of oxLDL ($p < 0.01$), which was further upregulated when co-treated with IL-1β and TNFα (2.87 ± 0.51 (oxLDL50) *vs.* 6.47 ± 1.28 (oxLDL50 + IL-1β + TNFα), $p < 0.0001$) (Fig. 5C and E). This is likely due to an increase in transcription of the oxLDL receptor mediated by inflammatory cytokines.[49] Similarly, an increase in SMC oxLDL uptake was observed for the migrated cells in the subendothelial layer (Fig. 5B and S7†). However, the amount of oxLDL uptake varied greatly for each SMC, making it difficult to quantify and compare between different conditions. SMC migration was not induced by low dose treatment of oxLDL (10 μg ml^{-1}), but was significantly upregulated when co-treated with cytokines ($p < 0.01$). Interestingly, high dose oxLDL (50 μg ml^{-1}) alone was sufficient to induce SMC migration based on the increase in migrated cell number (8.67 ± 5.51 (untreated) *vs.* 26.33 ± 7.37 (oxLDL50), $p < 0.05$) and mean migrated distance (42.7 μm (untreated) *vs.* 154.7 μm (oxLDL50), $p < 0.001$), with non-significant upregulation when co-treated with cytokines (Fig. 5F and S8†). These results suggested the importance of hyperlipidemia in SMC phenotypic modulation, which could induce strong SMC migratory effects with a similar potency to cytokines, reportedly through downregulation of genes encoding contractile protein and simultaneous activation of pro-inflammatory genes.[48,49] Overall, it was shown that a hyperlipidemic environment acted in concert with an inflammatory stimulus to trigger atherogenic events including inflammation-enhanced oxLDL uptake in ECs and phenotypic modulation of SMCs, representative of key disease progression pathways in atherosclerosis.[30,50]

Vitamin D and metformin attenuated cytokine-induced monocyte–EC adhesion and SMC migration

Vitamin D has been proposed to be an anti-atherogenic agent due to its protective effect against endothelial dysfunction[51] and SMC proliferation and migration.[18,52] Metformin, a first line anti-diabetic medication, also helps to reduce the risk of CVD through improving EC[53] and SMC function.[19,54] As most studies investigating vascular protective effects of vitamin D and metformin are carried out on 2D cultures of ECs and

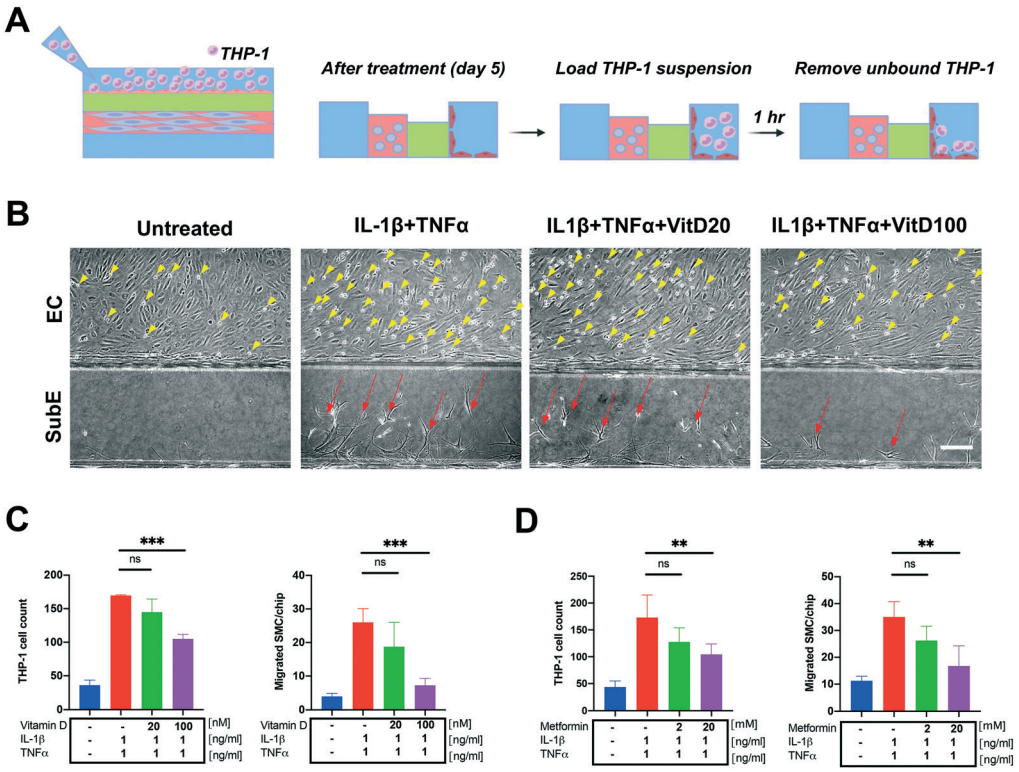

Fig. 6 Vitamin D and metformin attenuated monocyte–EC adhesion and SMC migration. (A) Experimental procedure for the on-chip monocyte adhesion assay. (B) Brightfield images of untreated, IL-1β (1 ng ml^{-1}) + TNFα (1 ng ml^{-1}) treated, IL-1β (1 ng ml^{-1}) + TNFα (1 ng ml^{-1}) + vitamin D (20 nM) treated, and IL-1β (1 ng ml^{-1}) + TNFα (1 ng ml^{-1}) + vitamin D (100 nM) treated chips after the monocyte adhesion assay. Yellow arrowheads indicate adhered THP-1 cells, red arrows indicate migrated SMCs. Scale bar: 200 μm. (C) Quantification of adhered THP-1 cells on ECs for vitamin D studies (left) (n = 3 chips from 3 independent experiments). Quantification of SMC migration into the subendothelial layer in terms of cell count for vitamin D studies (right) (n = 4 chips from 3 independent experiments). Results were expressed as mean ± SD. Data were analyzed with one-way ANOVA with Tukey's multiple comparison test (***$p < 0.001$, "ns" – not significant). (D) Quantification of adhered THP-1 cells on ECs for metformin studies (left) (n = 4–6 chips from 3 independent experiments). Quantification of SMC migration into the subendothelial layer in terms of cell count for metformin studies (right) (n = 4 chips from 3 independent experiments). Results were expressed as mean ± SD. Data were analyzed with one-way ANOVA with Tukey's multiple comparison test (**$p < 0.01$, "ns" – not significant).

SMCs separately, it is thus important to study their atheroprotective effects using a more physiological arterial wall model with co-cultured ECs and SMCs. Using our developed model, treatment of vitamin D (1*A*,25-dihydroxyvitamin D3) or metformin with inflammatory cytokines (IL-1β and TNFα) was performed for 48 hours, following which the changes in EC and SMC phenotype were examined. Besides characterizing SMC migration, monocyte adhesion to ECs, an early stage atherogenic event due to vascular inflammation, was also assessed on-chip by introducing monocytic THP-1 cells into the endothelialized channel (Fig. 6A). While a low level of vitamin D (20 nM) or metformin (2 mM) had negligible effects on THP-1 adhesion and SMC migration, we observed a significant reduction in both THP-1 adhesion and SMC migration with a higher dose of vitamin D (100 nM) or metformin (20 mM). Monocyte adhesion was decreased by 38% for vitamin D-treated chips (169.70 ± 1.16 (IL-1β + TNFα) *vs.* 105.00 ± 6.93 (IL-1β + TNFα + VitD100), $p < 0.001$), while a 40% decrease was observed for metformin-treated chips (173 ± 42.16 (IL-1β + TNFα) *vs.* 104.5 ± 19.28 (IL-1β + TNFα + metformin20), $p < 0.01$) (Fig. 6C and D). SMC migration was decreased by 72% in cell number for vitamin D-treated chips (26 ± 4.08 (IL-1β + TNFα) *vs.* 7.25 ± 2.06 (IL-1β + TNFα + VitD100), $p < 0.001$), and 52% for metformin-treated chips (35 ± 5.72 (IL-1β + TNFα) *vs.* 16.75 ± 7.5 (IL-1β + TNFα + metformin20), $p < 0.01$) (Fig. 6C and D). There were no significant differences in migration distance for both vitamin D and metformin studies (Fig. S9†). It should be noted that the inhibition of SMC migration could be due to mitigation of endothelial dysfunction or direct effects of vitamin D/metformin, or both, which warrants further investigation. Collectively, these results confirm the known atheroprotective effects of vitamin D and metformin through attenuating endothelial adhesion molecules and SMC migration during vascular inflammation in our co-culture model. These results also clearly demonstrated the applicability of the model for drug efficacy testing, which will be useful for identifying novel CVD drug candidates.

Discussion

In this work, we report a novel human arterial wall-on-a-chip which replicates key structural and biological aspects of the arterial intima–media interface including well-aligned and quiescent SMCs, and their phenotypic switching to a migratory state in response to ECM composition and pro-inflammatory factors in atherosclerosis. An important technical novelty is the dual-lane pillar-free gel confinement method used in our model that gave rise to the well-defined laminar structure similar to the multi-layered arterial wall. While microfluidic dual-lane pillar-based gel patterning has been reported previously, it has a discontinuous cell–ECM interface, which may subject cells to differential biomechanical cues and diffusive gradients.[55] Pillar-free gel confinement methods based on hydrophobic effects[56] or CBV effects[15,57] have been developed to pattern single-lane microchannels with continuous ECM side walls. Herein, we further engineered the CBV-based method to sequentially pattern 2 lanes of hydrogel adjacent to each other by fabricating 2 stepped heights. This enables us to create two continuous cell–ECM interfaces, and confers considerable flexibility to tune the ECM composition for the intima and media layers independently. Moreover, unlike the transwell model which is a top-down cell culture approach that adversely affects cell imaging, the design of the device represents the cross-section of the intima–media interface. This facilitates high quality imaging of both ECs and SMCs for real time monitoring of cellular morphologies and functions, cell–cell interaction, and cell–ECM interaction, which can help gain new insights into atherosclerosis and other vascular diseases.

As one of the main components of the cell niche, the ECM is known to mediate instructive signals for cell polarization, differentiation, and mobilization.[58] An important finding is the SMC phenotypic switching in response to ECM composition in the subendothelial layer. Although the subendothelial ECM is not in direct contact with the SMC, it clearly played a vital role in regulating the SMC phenotype by promoting cellular survival and growth, as well as retaining the quiescent phenotype. Going further, the well-aligned quiescent state of the SMC observed in our artery model is likely a synergistic outcome from the following four factors: serum starvation, co-culture with ECs, 3D culture in the collagen matrix, and the presence of a subendothelial layer rich in basement membrane-derived ECM proteins. These factors altogether served as a biomimetic microenvironment with physiological spatial guide and biochemical cues that were conducive to retaining SMCs in a quiescent state and their self-organization into densely packed layers.

SMC migration is a hallmark of cellular de-differentiation into a synthetic phenotype, and is known to drive the disease progression of atherosclerosis. Using our model, we can clearly observe and quantify single SMC migration into the subendothelial layer, which is not possible with existing conventional methods (scratch assay or transwell migration assay) or other EC–SMC co-culture platforms.[13–17] Moreover, we can potentially perform other assays to probe changes in cellular markers for migrated and non-migrated SMCs, which can provide more information on the SMC subpopulations. As demonstrated in the hyperlipidemia study, oxLDL can induce SMC migration into the intima. This finding is of major interest because high cholesterol is a well-established risk factor for CVD. This also provides a mechanistic insight on how oxLDL can affect SMC phenotypic modulation during early atherosclerosis. By testing the atheroprotective effects of vitamin D and metformin, we have shown that our 3D arterial wall model is potentially a powerful drug/therapeutic screening tool that can give novel insights on the synergistic cellular responses and interactions between ECs and SMCs.

Fluid shear stress plays a vital role in regulating vascular development, physiology and disease.[59,60] Disturbances in

blood flow may contribute to endothelial dysfunction and eventually lead to early and late stages of atherosclerosis.[61] As future work, development of a CBV-based curved intima–media interface is underway to construct the entire cross-section of the artery. This will allow for integration of mechanical stimuli such as shear stress for ECs and mechanical strain for SMCs. The outermost adventitia layer and other ECM components such as elastin that endows the tunica media with mechanical strength can also be incorporated into the chip with additional ECM layers.

Conclusions

In conclusion, we have developed a novel microfluidic EC–SMC co-culture platform that recapitulated several aspects of the human arterial intima–media interface for SMC migration studies in atherosclerosis. We also investigated how atherogenic factors modulate EC and SMC phenotypes, making this the first, to our knowledge, microengineered *in vitro* EC–SMC 3D co-culture model that allows the study of SMC migration at a single cell level. Noteworthily, we demonstrated the critical role of a basement membrane matrix-rich subendothelial layer in retaining the SMC quiescent phenotype, laying the groundwork for development of more physiological vascular tissue analogues for disease modeling, drug development and tissue engineering. Lastly, our ECM patterning technique for constructing a multi-layered structure is highly versatile, and can be further exploited to build other organ-like cellular microenvironments *in vitro*.

Author contributions

Chengxun Su: conceptualization, methodology, validation, formal analysis, investigation, data curation, writing – original draft, writing – review & editing, visualization. Nishanth Venugopal Menon: conceptualization, methodology, writing – review & editing. Xiaohan Xu: investigation, project administration. Yu Rong Teo: investigation, methodology. Huan Cao: investigation. Rinkoo Dalan: conceptualization, methodology, funding acquisition, writing – review & editing. Chor Yong Tay: conceptualization, resources, writing – review & editing. Han Wei Hou: conceptualization, methodology, visualization, supervision, resources, writing – original draft, writing – review & editing, project administration, funding acquisition.

Conflicts of interest

There are no conflicts to declare.

Acknowledgements

We would like to acknowledge financial support from the Singapore Ministry of Education Academic Research Fund Tier 1 (RG53/18) awarded to H. W. H., and National Medical Research Council (NMRC) Clinician Scientist Award (CSAINV17nov009) awarded to R. D. C. S. is supported by the NTU Interdisciplinary Graduate Programme Scholarship. H. C. is supported by the NTU Research Scholarship. We would like to thank Dr Chuah Yon Jin for the useful discussion on surface functionalization and providing the dopamine hydrochloride powder. We would like to acknowledge Prof Lena Ho for providing the human aortic endothelial cells. Schematics were created with BioRender.com.

References

1 WHO, *World Health Organization. Cardiovascular diseases (CVDs) Fact Sheet*, 2017.
2 H. C. Stary, A. B. Chandler, R. E. Dinsmore, V. Fuster, S. Glagov, W. Insull Jr., M. E. Rosenfeld, C. J. Schwartz, W. D. Wagner and R. W. Wissler, *Circulation*, 1995, **92**, 1355–1374.
3 P. Libby, J. E. Buring, L. Badimon, G. K. Hansson, J. Deanfield, M. S. Bittencourt, L. Tokgozoglu and E. F. Lewis, *Nat. Rev. Dis. Primers*, 2019, **5**, 56.
4 G. Pasterkamp, S. W. van der Laan, S. Haitjema, H. Foroughi Asl, M. A. Siemelink, T. Bezemer, J. van Setten, M. Dichgans, R. Malik, B. B. Worrall, H. Schunkert, N. J. Samani, D. P. de Kleijn, H. S. Markus, I. E. Hoefer, T. Michoel, S. C. de Jager, J. L. Bjorkegren, H. M. den Ruijter and F. W. Asselbergs, *Arterioscler., Thromb., Vasc. Biol.*, 2016, **36**, 1240–1246.
5 I. M. Stylianou, R. C. Bauer, M. P. Reilly and D. J. Rader, *Circ. Res.*, 2012, **110**, 337–355.
6 M. K. Ganesan, R. Finsterwalder, H. Leb, U. Resch, K. Neumuller, R. de Martin and P. Petzelbauer, *Tissue Eng., Part C*, 2017, **23**, 38–49.
7 J. J. Chiu, L. J. Chen, C. I. Lee, P. L. Lee, D. Y. Lee, M. C. Tsai, C. W. Lin, S. Usami and S. Chien, *Blood*, 2007, **110**, 519–528.
8 B. Imberti, D. Seliktar, R. M. Nerem and A. Remuzzi, *Endothelium*, 2002, **9**, 11–23.
9 A. S. Bulick, D. J. Munoz-Pinto, X. Qu, M. Mani, D. Cristancho, M. Urban and M. S. Hahn, *Tissue Eng., Part A*, 2009, **15**, 815–825.
10 T. Gong, K. Zhao, X. Liu, L. Lu, D. Liu and S. Zhou, *Small*, 2016, **12**, 5769–5778.
11 B. Yuan, Y. Jin, Y. Sun, D. Wang, J. Sun, Z. Wang, W. Zhang and X. Jiang, *Adv. Mater.*, 2012, **24**, 890–896.
12 S. N. Bhatia and D. E. Ingber, *Nat. Biotechnol.*, 2014, **32**, 760–772.
13 N. C. A. van Engeland, A. Pollet, J. M. J. den Toonder, C. V. C. Bouten, O. Stassen and C. M. Sahlgren, *Lab Chip*, 2018, **18**, 1607–1620.
14 P. Simmers, A. Gishto, N. Vyavahare and C. R. Kothapalli, *Tissue Eng., Part A*, 2015, **21**, 1455–1470.
15 N. V. Menon, H. M. Tay, S. N. Wee, K. H. H. Li and H. W. Hou, *Lab Chip*, 2017, **17**, 2960–2968.
16 Y. Zheng, J. Chen, M. Craven, N. W. Choi, S. Totorica, A. Diaz-Santana, P. Kermani, B. Hempstead, C. Fischbach-Teschl, J. A. López and A. D. Stroock, *Proc. Natl. Acad. Sci. U. S. A.*, 2012, **109**, 9342–9347.

17 A. Tan, K. Fujisawa, Y. Yukawa and Y. T. Matsunaga, *Biomater. Sci.*, 2016, **4**, 1503–1514.
18 E. Kassi, C. Adamopoulos, E. K. Basdra and A. G. Papavassiliou, *Circulation*, 2013, **128**, 2517–2531.
19 C. Driver, K. D. S. Bamitale, A. Kazi, M. Olla, N. A. Nyane and P. M. O. Owira, *J. Cardiovasc. Pharmacol.*, 2018, **72**, 121–127.
20 Y. Shin, S. Han, J. S. Jeon, K. Yamamoto, I. K. Zervantonakis, R. Sudo, R. D. Kamm and S. Chung, *Nat. Protoc.*, 2012, **7**, 1247–1259.
21 A. Milutinović, D. Šuput and R. Zorc-Pleskovič, *Bosnian J. Basic Med. Sci.*, 2020, **20**, 21–30.
22 E. Geiringer, *Am. Heart J.*, 1951, **41**, 359–368.
23 B. Martínez-González, M. D. C. Theriot-Girón, N. López-Serna, R. Morales-Avalos, A. Quiroga-Garza, C. G. Reyes-Hernández, A. Villanueva-Olivo, J. I. Leyva-Villegas, A. Soto-Domínguez, D. de la Fuente-Villarreal, R. E. Elizondo-Omaña and S. Guzmán-López, *Int. J. Morphol.*, 2015, **33**, 1205–1212.
24 K. Nakagawa and Y. Nakashima, *Atherosclerosis*, 2018, **274**, 235–242.
25 Y. Nakashima, Y. X. Chen, N. Kinukawa and K. Sueishi, *Virchows Arch.*, 2002, **441**, 279–288.
26 H. K. Kleinman and G. R. Martin, *Semin. Cancer Biol.*, 2005, **15**, 378–386.
27 K. Murata, T. Motayama and C. Kotake, *Atherosclerosis*, 1986, **60**, 251–262.
28 J. A. Eble and S. Niland, *Curr. Pharm. Des.*, 2009, **15**, 1385–1400.
29 M. K. O'Connell, S. Murthy, S. Phan, C. Xu, J. Buchanan, R. Spilker, R. L. Dalman, C. K. Zarins, W. Denk and C. A. Taylor, *Matrix Biol.*, 2008, **27**, 171–181.
30 R. Ross, *Am. Heart J.*, 1999, **138**, S419–S420.
31 M. R. Alexander and G. K. Owens, *Annu. Rev. Physiol.*, 2012, **74**, 13–40.
32 K. P. Dingemans, P. Teeling, J. H. Lagendijk and A. E. Becker, *Anat. Rec.*, 2000, **258**, 1–14.
33 M. W. Peters, P. B. Canham and H. M. Finlay, *J. Vasc. Res.*, 1983, **20**, 221–233.
34 A. J. Engler, S. Sen, H. L. Sweeney and D. E. Discher, *Cell*, 2006, **126**, 677–689.
35 R. G. Wells, *Hepatology*, 2008, **47**, 1394–1400.
36 H. Cao, M. K. H. Lee, H. Yang, S. K. Sze, N. S. Tan and C. Y. Tay, *Langmuir*, 2019, **35**, 7487–7495.
37 J. Thyberg and A. Hultgardh-Nilsson, *Cell Tissue Res.*, 1994, **276**, 263–271.
38 X. Li, P. Tsai, E. D. Wieder, A. Kribben, V. Van Putten, R. W. Schrier and R. A. Nemenoff, *J. Biol. Chem.*, 1994, **269**, 19653–19658.
39 U. Hedin, B. A. Bottger, E. Forsberg, S. Johansson and J. Thyberg, *J. Cell Biol.*, 1988, **107**, 307–319.
40 A. W. Orr, M. Y. Lee, J. A. Lemmon, A. Yurdagul Jr., M. F. Gomez, P. D. Bortz and B. R. Wamhoff, *Arterioscler., Thromb., Vasc. Biol.*, 2009, **29**, 225–231.
41 E. Hergenreider, S. Heydt, K. Treguer, T. Boettger, A. J. Horrevoets, A. M. Zeiher, M. P. Scheffer, A. S. Frangakis, X. Yin, M. Mayr, T. Braun, C. Urbich, R. A. Boon and S. Dimmeler, *Nat. Cell Biol.*, 2012, **14**, 249–256.
42 M. F. Fillinger, S. E. O'Connor, R. J. Wagner and J. L. Cronenwett, *J. Vasc. Surg.*, 1993, **17**, 1058–1067 discussion 1067-1058.
43 P. Libby, *J. Am. Coll. Cardiol.*, 2017, **70**, 2278–2289.
44 S. E. Goldblum, B. Hennig, M. Jay, K. Yoneda and C. J. McClain, *Infect. Immun.*, 1989, **57**, 1218–1226.
45 E. Fahey and S. L. Doyle, *Front. Immunol.*, 2019, **10**, 1426.
46 N. Auge, V. Garcia, F. Maupas-Schwalm, T. Levade, R. Salvayre and A. Negre-Salvayre, *Arterioscler., Thromb., Vasc. Biol.*, 2002, **22**, 1990–1995.
47 Y. Kiyan, S. Tkachuk, D. Hilfiker-Kleiner, H. Haller, B. Fuhrman and I. Dumler, *J. Mol. Cell. Cardiol.*, 2014, **66**, 72–82.
48 N. A. Pidkovka, O. A. Cherepanova, T. Yoshida, M. R. Alexander, R. A. Deaton, J. A. Thomas, N. Leitinger and G. K. Owens, *Circ. Res.*, 2007, **101**, 792–801.
49 D. P. Hajjar and M. E. Haberland, *J. Biol. Chem.*, 1997, **272**, 22975–22978.
50 A. C. Doran, N. Meller and C. A. McNamara, *Arterioscler., Thromb., Vasc. Biol.*, 2008, **28**, 812–819.
51 M. Martinesi, S. Bruni, M. Stio and C. Treves, *Cell Biol. Int.*, 2006, **30**, 365–375.
52 A. R. Menezes, M. C. Lamb, C. J. Lavie and J. J. DiNicolantonio, *Curr. Opin. Cardiol.*, 2014, **29**, 571–577.
53 A. Nafisa, S. G. Gray, Y. Cao, T. Wang, S. Xu, F. H. Wattoo, M. Barras, N. Cohen, D. Kamato and P. J. Little, *Pharmacol. Ther.*, 2018, **192**, 150–162.
54 M. Deng, D. Su, S. Xu, P. J. Little, X. Feng, L. Tang and A. Shen, *Front. Pharmacol.*, 2020, **11**, 635.
55 G. Adriani, D. Ma, A. Pavesi, R. D. Kamm and E. L. K. Goh, *Lab Chip*, 2017, **17**, 448–459.
56 S. Han, J. Kim, R. Li, A. Ma, V. Kwan, K. Luong and L. L. Sohn, *Adv. Healthcare Mater.*, 2018, **7**, 1800122.
57 S. J. Trietsch, G. D. Israëls, J. Joore, T. Hankemeier and P. Vulto, *Lab Chip*, 2013, **13**, 3548–3554.
58 C. Frantz, K. M. Stewart and V. M. Weaver, *J. Cell Sci.*, 2010, **123**, 4195.
59 K. Tanaka, D. Joshi, S. Timalsina and M. A. Schwartz, *Cytoskeleton*, 2021, 1–15.
60 S.-I. Murtada, Y. Kawamura, G. Li, M. A. Schwartz, G. Tellides and J. D. Humphrey, *Dev. Dyn.*, 2020, 629–639.
61 S. Baratchi, K. Khoshmanesh, O. L. Woodman, S. Potocnik, K. Peter and P. McIntyre, *Trends Mol. Med.*, 2017, **23**, 850–868.